Petroleum Science 20 (2023) 3131–3142

Contents lists available at ScienceDirect

Petroleum Science

journal homepage: www.keaipublishing.com/en/journals/petroleum-science

Original Paper

Micro-macro fracture mechanism of heterogeneous granite in percussive drilling

Wei-Ji Liu [a, b, *], Yan-Fei Wang [a], Zhao-Wang Dan [c], Xiao-Hua Zhu [a, b]

[a] School of Mechatronic Engineering, Southwest Petroleum University, Chengdu, 610500, Sichuan, China
[b] Geothermal Energy Research Center, Southwest Petroleum University, Chengdu, 610500, Sichuan, China
[c] Powerchina Sinohydro Bureau 7 Co., LTD, Chengdu, 610500, Sichuan, China

ARTICLE INFO

Article history:
Received 12 October 2022
Received in revised form
3 February 2023
Accepted 5 May 2023
Available online 6 May 2023

Edited by Jia-Jia Fei

Keywords:
Percussive drilling
PFC
Rock fragmentation characteristics
Rock breaking efficiency

ABSTRACT

The conventional rotary rock breaking method faces a technical bottleneck in improving the rate of penetration (ROP) in deep hard formations. Percussive drilling is the most potential approach to increase rock-breaking efficiency and ROP. However, the rock-breaking mechanism of percussive drilling is still unclear enough, especially the micro-fracture mechanism of rock under confining pressure (under lateral pressure and hydraulic pressure). In this paper, the impact rock breaking experiments by four kinds of Polycrystalline Diamond Compact (PDC) cutters are carried out using a drop-weight impact testing machine and an acoustic emission (AE) recording system, the influence of parameters such as cutter shape, rake angle, and impact energy on rock-breaking are systematically analyzed. This study includes a numerical simulation to examine the process of crack initiation, propagation, and cuttings formation during the impact process with the consideration of confining pressure. The results show the conical-shaped cutter is the most aggressive with high breaking efficiency. The penetration depth of the cutter is mainly influenced by the impact energy and cutter shape than the rake angle of the cutter. There exists critical impact energy makes the rock breaking efficiency the highest. The critical impact energy is about 40 J when using the conical-shaped cutter with a rake angle of 15°. The rock mainly failed in tensile mode, and the inter-grain crack is the main crack. Hydraulic pressure can inhibit the formation of horizontal cracks, while lateral pressure can inhibit the formation of vertical cracks and reduce the proportion of tensile cracks. The research results can provide some reference and basis for improving the rock-breaking efficiency in deep hard formations.

1. Introduction

The deep oil and gas resources accounted for the majority of the growth in global proved oil and gas reserves in the past decade, and the deep formations have become the replacement field for oil and gas storage and production (Zhu et al., 2022). With the development of oil and gas exploration towards the deep formations, high strength, high hardness, and high plasticity become the main factors affecting the drilling cost and drilling efficiency (Yang et al., 2018; Zhu et al., 2019), and traditional mechanical rock breaking methods encounter serious problems. Percussive drilling is the most effective drilling method to improve the ROP in deep hard formations (Saksala et al., 2018).

To increase the rock-breaking energy of the drill bit and improve rock-breaking efficiency in deep hard formations, percussive drilling has emerged. According to previous studies, percussive drilling can significantly increase the ROP and reduce bit wear (Li et al., 2020; Pavlovskaia et al., 2015). Several types of percussive drilling tools have been developed over the past few decades, which can be divided into rotary percussion drilling tools, torsional percussion drilling tools, and rotary-torsional percussion drilling tools (Xi et al., 2022; Liu et al., 2018b). The percussive drilling method using rotary percussion drilling tools is called rotary percussive drilling, which is the most widely used drilling method (Oparin et al., 2022). Many studies have been performed to understand rock-breaking mechanisms under impact loads. The rock-breaking efficiency is closely related to the cutter shape, weight on bit (WOB),

* Corresponding author. School of Mechatronic Engineering, Southwest Petroleum University, Chengdu, 610500, Sichuan, China.
E-mail address: Lwj2017_swpu@163.com (W.-J. Liu).

https://doi.org/10.1016/j.petsci.2023.05.002

impact energy, lateral pressure, and hydraulic pressure (Ajibose et al., 2015; Tan et al., 1998). Aldannawy et al. (2021) studied the effect of cutter shape on the impact breaking of hard rock through experiments, which provided a reference for the optimization of drill cutter in hard formations. One of the advantages of percussive drilling is that the demand for WOB is small, but there is also an optimal WOB that maximizes rock-breaking efficiency. Song et al. (2021) believed that this is due to the dependence of the pseudo-stiffness of the bit-rock interface on the WOB. Impact energy is the most important factor affecting rock-breaking efficiency (Jiang et al., 2020). Saksala et al. (2014) studied the fracture of granite under different impact energies of multi-cutters experimentally, focusing on the volume of cuttings. Under lateral pressure and hydraulic pressure (under confining pressure), the strength of the rock increases, the failure mode of the rock will change from ductile to brittle, and the ROP decreases, which has a great influence on the rock breaking (Liu et al., 2018a; Meng et al., 2015, 2021; Saadat et al., 2021). Du et al. (2020), Li et al. (2021), and Song et al. (2022) conducted a dynamic indentation test on granite under lateral pressure and identified the rock failure mode (tensile failure or shear failure) by observing the shape of cracks. Based on the isotropic damage model, Saksala (2016) carried out dynamic indentation tests on a hard rock under confining pressure using drill bits. However, the model can't well simulate the process of crack propagation. Due to the challenging downhole environment, the rock-breaking mechanism of percussive drilling is still not clear enough, especially the initiation, propagation, and connection mechanism of micro-fracture.

This paper presents an experimental study of hard rock impacted with a single PDC cutter using a drop-weight impact testing machine and an AE monitoring system, and the cutter shape, rake angle, and impact energy are optimized under atmospheric pressure. This study also includes a numerical simulation to examine the process of crack initiation, propagation, and cuttings formation from grain scale during the impact process with the consideration of confining pressure and heterogeneity of rocks. The research results provide the theoretical basis for further understanding of rock impact-breaking mechanisms and optimization of rock impact-breaking parameters.

2. Experiment of granite impacted with a single PDC cutter

2.1. Engineering model

During rotary percussive drilling, the top drive system provides torque for the drill string and drives the drill bit to break rock. Drilling fluid provides energy for the hammer, the hammer applies high-frequency impact loads to the bit through energy conversion, developing craters surrounded by cracks beneath the cutter, and the dense zone is located below the craters (Ji et al., 2021; Liu et al., 2008), as shown in Fig. 1. The study of rock fragmentation mechanism under single PDC cutter is the basis for analyzing the fragmentation mechanism in percussive drilling (Aldannawy et al., 2021; Xi et al., 2022; Zhu et al., 2019). In this study, a PDC cutter is selected as the test object.

2.2. Experimental scheme

To study the impact rock breaking characteristics under different cutter shapes, in this study, the single cutter impact rock experiment is carried out using a drop-weight impact testing machine. The rock sample is a cylinder with a diameter of 50 mm and a height of 50 mm (quarried in Hubei Province, China). The elastic modulus, uniaxial compressive strength (UCS), and tensile strength are 21.5 GPa, 117.4 MPa, and 9.11 MPa, respectively. The rock is placed directly under the PDC cutter, and the sides of the rock are bolted to prevent it from moving during the test.

The PDC cutter is interference connected with the drop hammer through the pin, and the rake angle of the cutter can be adjusted by changing the position of the pin. In this study, the rake angle (γ) is defined as the angle between the central axis of the cutter and the vertical line. The four kinds of PDC cutters used in the test are shown in Fig. 2. Before the experiment, the weight of the drop hammer and the cutter are measured to be 8.83 kg. In the experiment, the drop hammer and the cutter are raised to a certain height to release and make a free-fall movement to impact the rock, the AE signal is recorded by the AE monitoring system to monitor the microcrack development of the rock.

After the test, immerse the sample in water. After the rock has fully absorbed water, remove it from the water and dry the rock surface with a napkin. Then use a syringe to fill the crater with water and calculate its volume by measuring the amount of water used. The diameter of the crater is approximately measured with a steel ruler, and the depth of the crater is measured with a vernier caliper.

3. Experimental results and discussion

3.1. Effect of cutter shapes

The morphology of craters at different cutter shapes with a rake angle of 15° is demonstrated in Fig. 3. The red line in the figure indicates the impact position and the black line indicates the outline of the impact crater. The surfaces of these craters show two kinds of morphologies. Under tensile failure, the surface of the crater is relatively rough, while the crater surface under shear failure is smoother due to the squeezing and shearing of the cutter (Teng et al., 2023). The impact-breaking rock debris is powdery and blocky, and a dense area is formed under the impact position. It is worth mentioning that the impact of the conical-shaped cutter on the granite produced petal-shaped chips and left black wear marks.

With the increase of impact energy, the rock breaking volume increases exponentially, and the penetration depth increases in a fluctuating manner due to the rock heterogeneity, as shown in Fig. 4. The ductile failure mode of rock occurs when the impact energy is small, as shown in Fig. 4(a) and the contact area between the PDC cutter and the rock is small, the cutter shape has little effect on rock breaking. With the increase in impact energy, the shape of the cutter has an increasing influence on rock breaking. Among the four kinds of the cutter, the conical-shaped cutter is the most aggressive with high breaking efficiency.

Although the cutting volume, penetration depth, and crack propagation can reflect the rock-breaking efficiency of the cutter, mechanical specific energy (MSE) is the most important parameter to characterize the rock-breaking efficiency (Hustrulid and Fairhurst, 1971). MSE is defined as the energy consumed to break per unit volume of rock, namely:

$$\mathrm{MSE} = \frac{W}{V} \tag{1}$$

where W is the total energy consumed by rock breaking (J); V is the volume of cuttings (mm^3).

To find the optimal impact energy for rock breaking with different cutter shapes, we explored the relationship between MSE and impact energy. Fig. 5 displays the curves of MSE versus energy under different cutter shapes. It shows a non-linear relationship between rock-breaking efficiency and impact energy. The rock-breaking efficiency of the Three-blade cutter, Ax-shaped cutter, and the cylindrical cutter is the best under a small impact energy

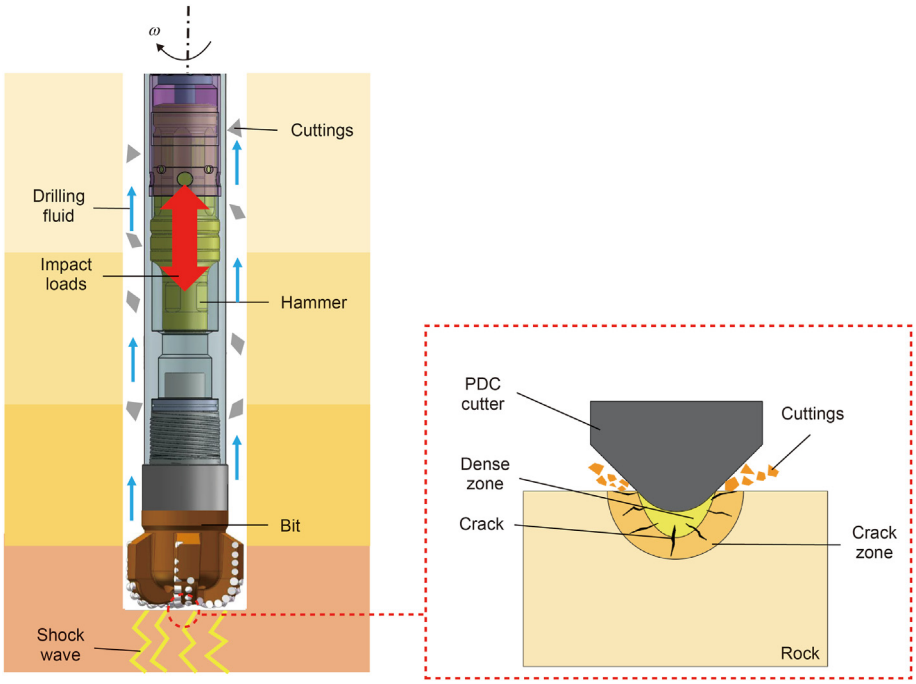

Fig. 1. Engineering model.

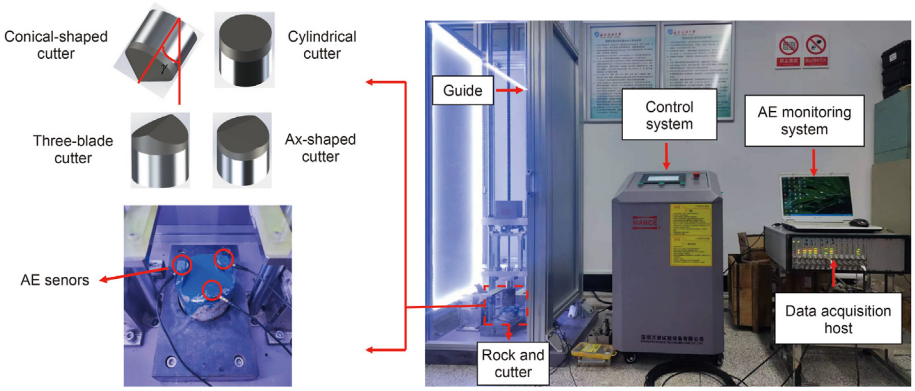

Fig. 2. Single cutter impact rock breaking setup.

(10 J), while the conical-shaped cutter is more suitable for high impact energy, which is mainly determined by the radius of curvature of the cutter. Conical-shaped cutter has a small radius of curvature, and when the impact energy is insufficient, most of the energy is consumed in compacting the rock. Among the four kinds of cutters, the Ax-shaped cutter has the lowest rock-breaking efficiency.

We selected rock samples impacted by a conical-shaped cutter with 60 J energy for three-dimensional profile scanning, as shown in Fig. 6. It can be seen that a conical crater is formed under the cutter, and cracks appear around the crater, and the cracks have not been completely connected, as shown in the blue part in Fig. 6(a). It is more convenient to see the crack distribution from the cross-section, as shown in Fig. 6(b)–(d).

3.2. Effect of rake angle

In this section, rock-breaking tests with different rake angles are carried out with the conical-shaped cutter. Fig. 7 shows the rock-breaking efficiency of granite impacted by the conical-shaped cutter at a rake angle of 0°–15°. It can be seen that the rake angle also has a great influence on the fragmentation of granite. Because of the rock heterogeneity, the rock-breaking efficiency is not the highest when the rake angle of the cutter is 0°. With the increase of the rake angle, the variation of MSE shows great randomness. In addition, with the increase of energy, limited by the size of the rock sample, the rock sample has been fractured before MSE shows obvious regular change with impact energy. In terms of penetration depth, the rake angle is far less important than the cutter shape and impact energy.

3.3. Acoustic emission response during impact

The acoustic emission (AE) recording system used in the study is the Vallen AMSY-6 system with a frequency of 10 MHz, and the amplifier gain and trigger threshold value of the system is 40 dB. The AE count refers to the number of times that the pulse signal crosses the threshold during the test time, which reflects the

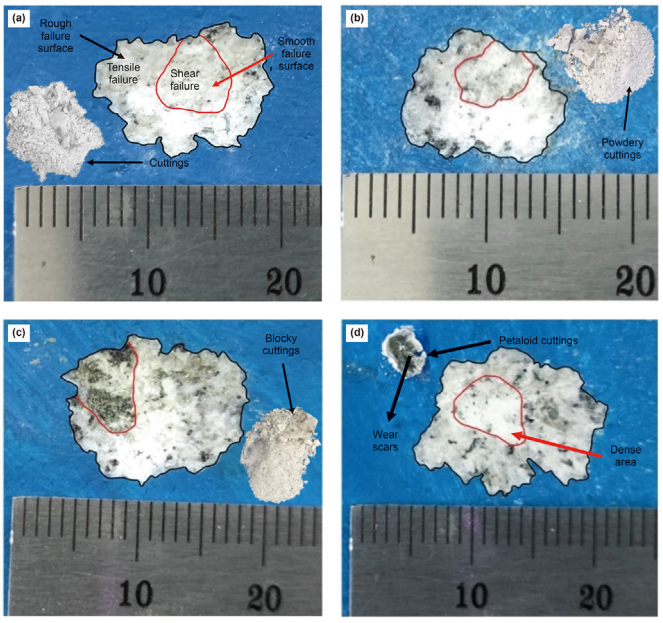

Fig. 3. Morphology of the crater after impact. (**a**) Three-blade cutter 15° 40 J, (**b**) Ax-shaped cutter 15° 40 J, (**c**) Cylindrical cutter 15° 40 J, (**d**) Conical-shaped cutter 15° 40 J.

intensity of the signal in the process of rock failure and can reveal the law of rock failure caused by the expansion of microscopic defects (Wang et al., 2021a). Other AE parameters, including rise time, duration time, and maximum amplitude are shown in Fig. 8. The cumulative AE counts can reflect the evolution of rock damage, and the increase of the value indicates the increase of rock damage.

AE signals were collected in impact rock-breaking tests for the conical-shaped cutter and common cylindrical cutter. Fig. 9 shows the change of AE counts with time during the impact of two kinds of cutters at 60 J energy. It can be seen that the AE counts increase sharply at the moment when the cutter hits the rock. The cumulative AE counts of the conical-shaped cutter impacting granite are obviously higher than that of the cylindrical cutter, which also reflected the advantages of the conical-shaped cutter in rock breaking. There are two peaks in the AE counts curve of the cylindrical cutter, which is caused by the rebound of the cutter after hitting the rock and then hitting the rock again.

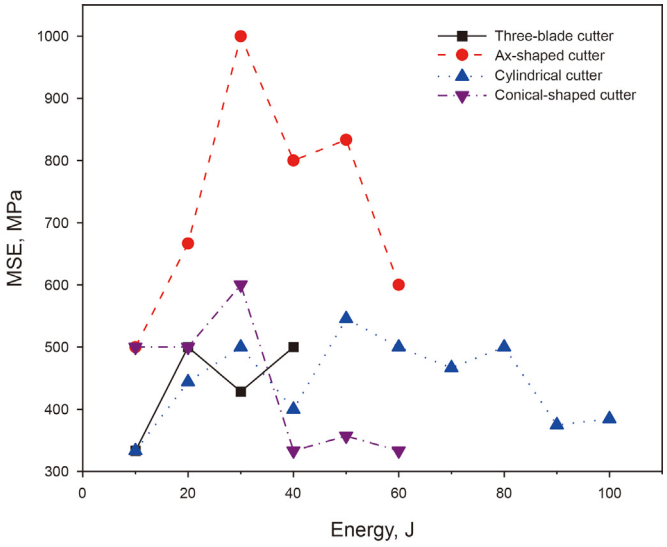

Fig. 5. MSE under different impact energies and cutter shapes.

Researchers found that the distribution of AF (ratio of AE counts to duration time)- RA (ratio of rise time to maximum amplitude) can distinguish tensile cracks from shear cracks, as shown in Fig. 10 (Zhao et al., 2022). The transition line divides the crack into two parts, above the transition line are tensile cracks, and below it are shear cracks. The value of the slope of the transition line is related to the structure and properties of the rock. Jiang et al. (2022) suggested that the slope should be taken as 90 in the Brazilian splitting test (BST) of granite, and the value was also adopted in this study.

Fig. 11 shows the AE RA - AF scatter plot for the process of granite fracture. It can be seen that the cracks are mainly tensile, and the proportion of tensile cracks generated by the cylindrical cutter impacting granite is larger than that of the conical-shaped cutter.

4. Numerical simulation of single cutter impact rock breaking

The two-dimensional particle flow code (PFC) based on the discrete element method (DEM) has become an important tool to investigate the rock impacting mechanism, it has great advantages

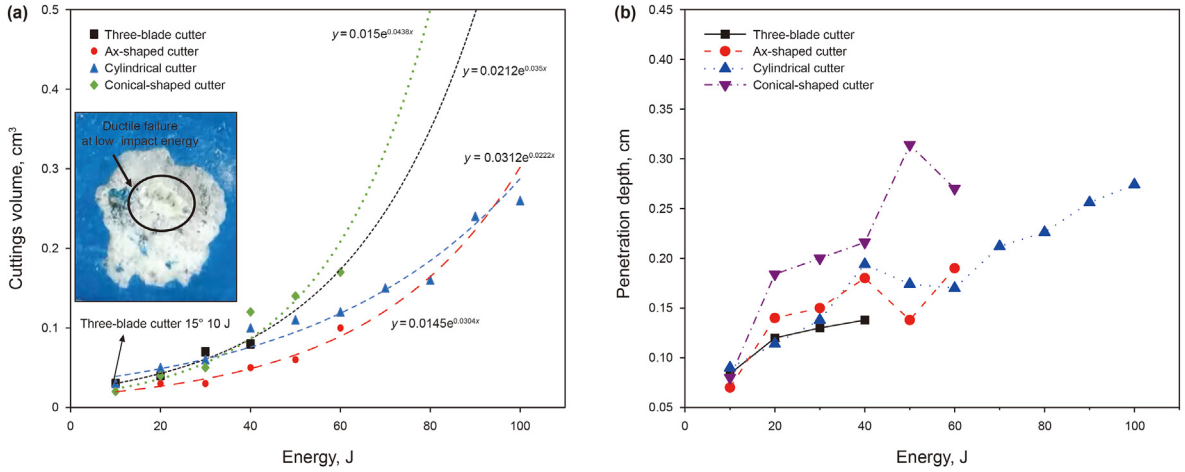

Fig. 4. Rock breaking efficiency under different cutter shapes. (**a**) Cuttings volume under different impact energies and cutter shapes, (**b**) Penetration depth under different impact energies and cutter shapes.

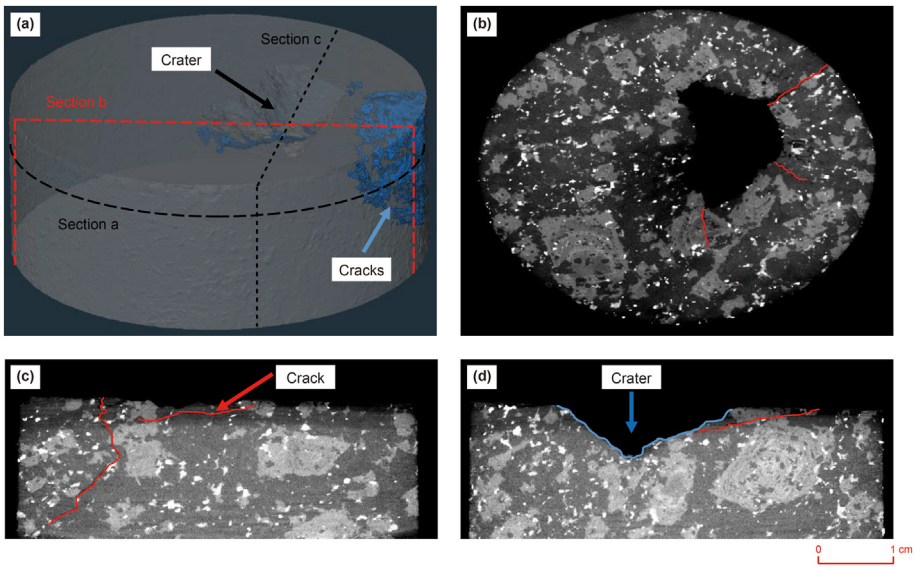

Fig. 6. Three-dimensional profile characteristics of the crater and cracks produced by conical-shaped cutter impacting rock under 60 J energy. (**a**) Three-dimensional profile characteristics, (**b**)Section a, (**c**) Section b, (**d**) Section c.

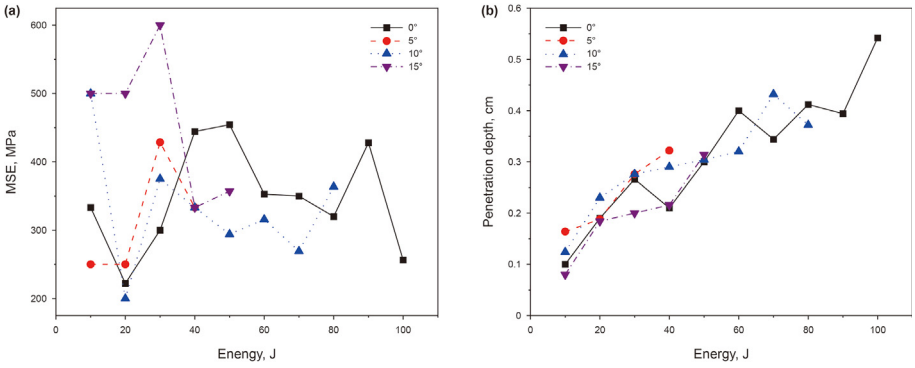

Fig. 7. Rock breaking efficiency of a conical-shaped cutter under different rake angles. (**a**) MSE under different impact energies and rake angles, (**b**) Penetration depth under different impact energies and rake angles.

in simulating the process of crack propagation and rock chips formation (Han et al., 2018; Huang et al., 2019). PFC has built-in rich contact models, such as Linear Parallel Bond Model (PBM) and smooth-joint Model (SJM). Grain-based mode (GBM) (Bahrani et al., 2014) is a combination of PBM and SJM. The internal grain is constructed by PBM and SJM is used to simulate the bond between grains, which can well reflect the damage behavior of heterogeneous granite (Tan et al., 2021). However, since SJM allows particles to pass through each other after the connection is broken (Potyondy and Cundall, 2004; Wang et al., 2021b; Zhao et al., 2021), as shown in Fig. 12, GBM performs poorly in mimicking the crushing behavior of rocks under impact. Thus, we developed an extended PBM (E-PBM) to reconstruct the rock model.

4.1. Establishment of heterogeneous hard rock model

To establish the heterogeneous E-PBM of granite, it is necessary to extract the grain boundaries of the granite. Use the camera to obtain a digital image, then change the brightness to identify the shape of the mineral particles, and finally get the grain boundaries of the granite, as shown in Fig. 13.

Based on the grain boundaries of granite, the granite characterization model based on E-PBM was established. Firstly, a rectangular rock sample with a height of 50 mm and a width of 25 mm was generated, and the contact between particles was constructed with PBM. Then, the extracted grain boundaries of granite were imported into the PBM, grouped by mineral components, and the rock model containing four minerals was generated. Subsequently, the contacts at the grain boundaries were identified and re-assigned to simulate the bonding between grains. Thus, the E-PBM characterization model of granite was established, as shown in Fig. 14.

4.2. Calibration procedure

The model was calibrated by uniaxial compression test (UCT) and BST. The macroscopic mechanical parameters of granite were used for calibrating the model parameters, and a large number of numerical simulations will be conducted to match the physical parameters. The simulation results are shown in Fig. 15.

It can be seen that the number of cracks increases exponentially, “oa” was the compaction stage of the rock, and no cracks were generated in this stage. At point “a”, the rock entered the yielding stage and produced cracks. In stage “bc”, the expanding cracks connected, ultimately leading to rock fracture. The microscopic parameters of granite at normal temperature are shown in Table 1.

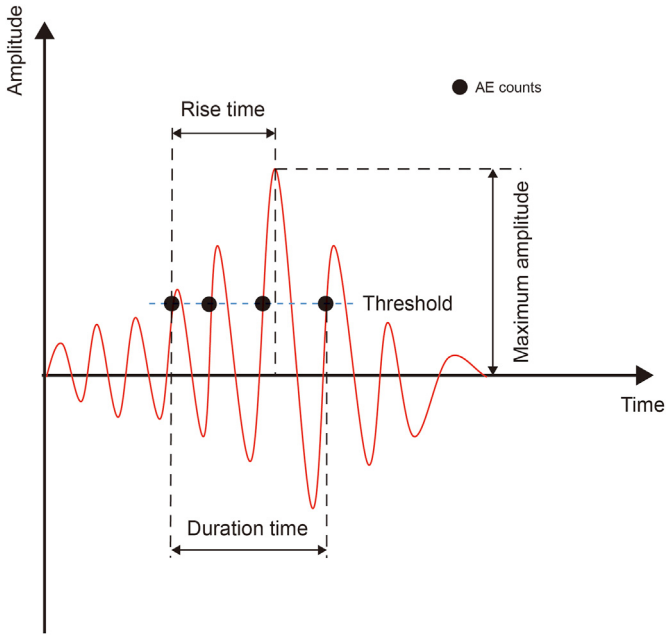

Fig. 8. AE parameters.

The numerical simulation results agree closely with the experimental results, with an error of about 5%, as shown in Table 2. Therefore, the calibrated parameters can simulate the mechanical behavior of granite.

4.3. Establishment of single cutter impact rock breaking model

In PFC, the motion of the wall does not obey Newton's laws of motion and force-displacement law but is defined by the user. Therefore, walls are not suitable for constructing PDC cutters. In this study, the PDC cutter is composed of a rigid cluster (clump) based on the profile of a conical-shaped cutter. The clump will not be deformed or destroyed, and it follows Newton's laws of motion and force-displacement law.

The impact energy is simulated by applying initial velocity to the cutter. The weight of the cutter in the simulation is set to be the same as that of the hammer and cutter in the experiment-8.83 kg, and the rake angle is 15°. Lateral pressure is simulated by applying forces on the left and right walls. To simulate the effect of hydraulic pressure, a flexible boundary is generated on the upper part of the rock, a force is applied to the flexible boundary, and the particles close to the wall are set as non-reflective boundaries, as shown in Fig. 16.

5. Numerical simulation results and discussions

In PFC, the number of cuttings and cracks can be detected and recorded, the volume of the total cuttings is V, and V_i is the volume of single cuttings, then the total cuttings volume V can be expressed as:

$$V = \sum_{1}^{n_c} V_i \tag{2}$$

where n_c is the number of cuttings.

In the simulation procedure, tensile crack and shear crack will be generated due to the different failure modes. The total number of cracks generated is denoted as n, where the number of tensile cracks is n_t, the number of shear cracks is n_s, and the proportion of tensile cracks is defined as k:

$$n = n_t + n_s \tag{3}$$

$$k = \frac{n_t}{n} \times 100\% \tag{4}$$

The number of cracks per unit is defined as the number of cracks generated per unit volume of cuttings and is represented by m:

$$m = \frac{n}{V} \tag{5}$$

The value of m can reflect the rock-breaking efficiency, and the smaller m is, the higher the rock-breaking efficiency is.

The crack length can also reflect the rock-breaking efficiency. The length of a single crack is denoted as l_i, the angle between the crack and the horizontal plane is α, and the equivalent radial crack length is defined as the projection length of the crack along the radial direction and is denoted as L_r:

$$L_r = \sum_{1}^{n} l \times \cos\alpha - \sum_{2}^{n} l_o \tag{6}$$

where l_o is the overlap length of cracks in the radial direction.

5.1. Rock breaking mechanism under different impact energy

Fig. 17 shows the impact rock breaking without confining pressure under different impact energies. According to the location and failure mode of cracks, four kinds of cracks were generated in the simulation procedure. They are intragranular shear crack, intragranular tensile crack, intergranular shear crack, and intergranular tensile crack. With the increase of impact energy, L_r increases, but the magnitude of the increase decreases, which is mainly caused by the repeated fragmentation of cuttings. In

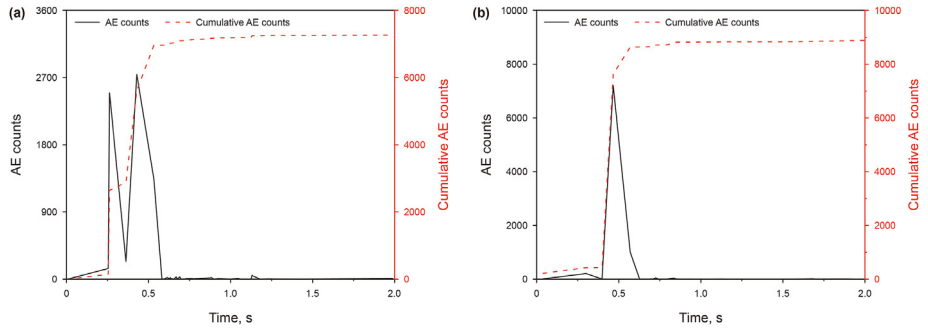

Fig. 9. The Curves of AE counts and cumulative AE count with time. (**a**) Cylindrical cutter with a rake angle of 15°, (**b**) Conical-shaped cutter with a rake angle of 15°.

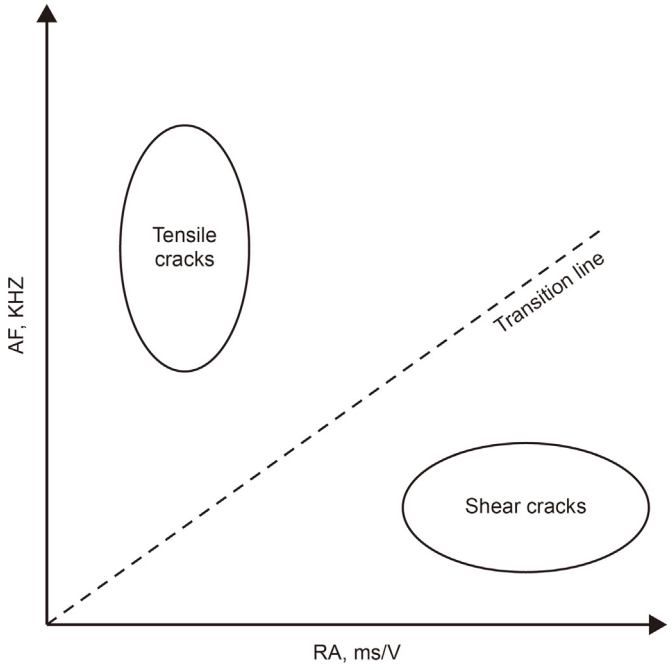

Fig. 10. Criteria for fracture classification in AE.

addition, the volume of cuttings increases greatly due to the transverse crack connection, as shown in Fig. 17(f). Under high impact energy, a conical impact crater was formed and produced powdery cuttings, as shown in Fig. 17(i). The rock mainly fails in tensile mode, which is the same as the experimental result. With the increase of impact energy, k changes little. When the energy is less than 40 J, with the increase of impact energy, MSE decreases, and then the amplitude decreases and finally tends to be stable, indicating that 40 J is the critical impact energy for rock breaking. The variation trend of m is similar to that of MSE, as shown in Fig. 18, indicating that it is reasonable to use m to evaluate the rock-breaking efficiency.

The fracture system in the rock under the impact, as extracted from the displacement of the particle, is illustrated in Fig. 19(a). Underneath the cutter locates the damaged zone, due to the rake angle of the cutter and the heterogeneity of the rock, the damaged zone is irregular. The rock on the inclined side of the cutter undergoes compression while tension cracks are generated on the other side, ultimately forming cuttings. A dense zone surrounded by the cracked zone is located below the cuttings.

In the process of the cutter impacting rock, the speed of the cutter changes parabolically, the number of cracks and cuttings volume change exponentially, and the volume of the cutting changes slightly slower than the number of cracks. The impact force gradually increases with the movement of the cutter, and decreases sharply after reaching the maximum value, as shown in Fig. 19(b), and the number of cracks and cuttings volume increase sharply during the reduction of impact force, which is similar to Saadati's study (Saadati et al., 2020).

5.2. Effect of lateral pressure on the rock-breaking mechanism

Fig. 20 shows the crushing results of granite impacted by the cutter with an energy of 60 J under different lateral pressures. It can be seen that L_r decreases with the increase of lateral pressure, which means that the radial crack propagation is suppressed. In

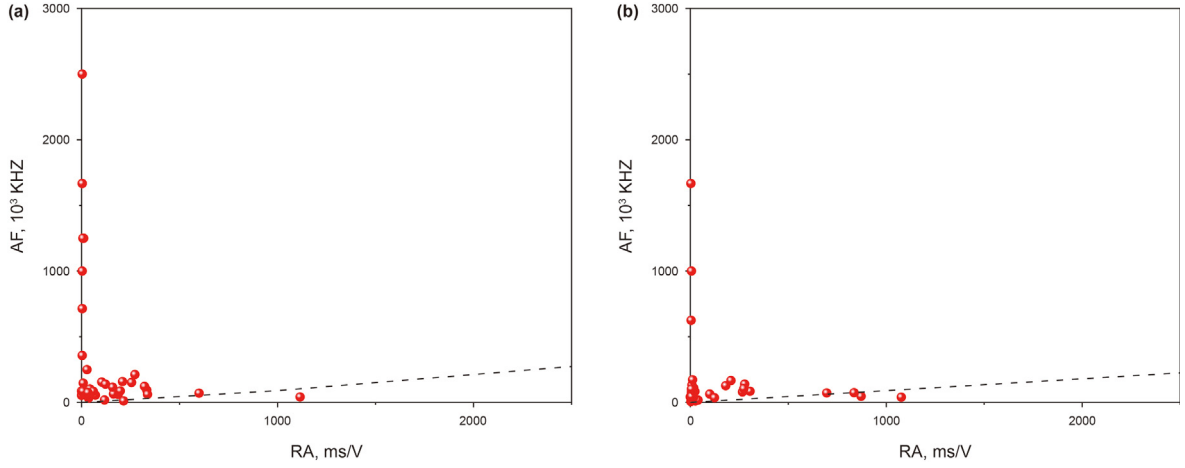

Fig. 11. Scatter plot of AE AF-RA during granite fracture. (**a**) conical-shaped cutter with a rake angle of 15° and energy of 60 J, (**b**) cylindrical cutter with a rake angle of 15° and energy of 60 J.

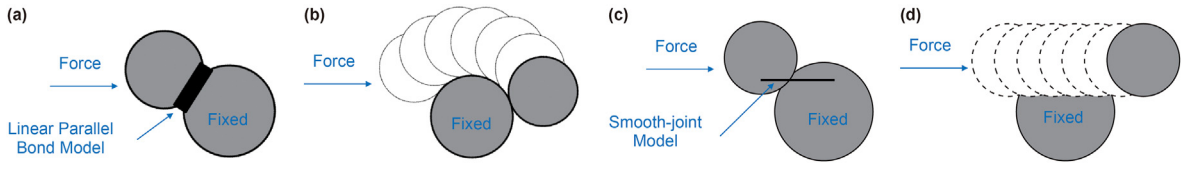

Fig. 12. The failure of PBM and SJM (Bahrani et al., 2014).

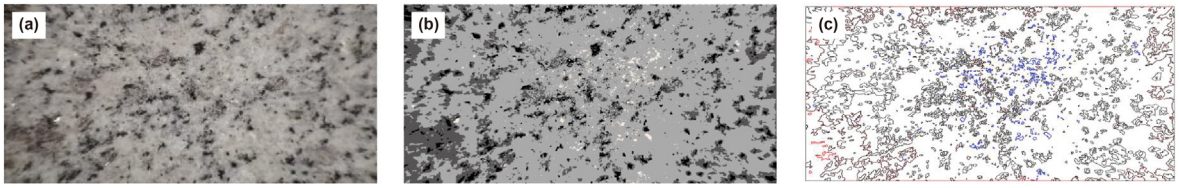

Fig. 13. Grain boundaries acquisition. (**a**) Image of granite, (**b**) Image after changing brightness, (**c**) Grain boundaries.

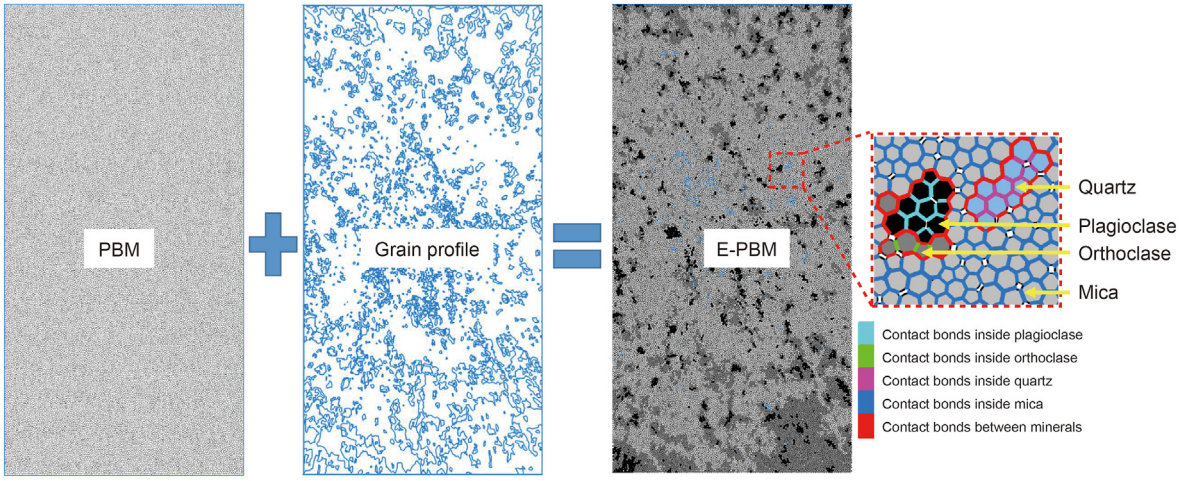

Fig. 14. The generation procedure of E-PBM.

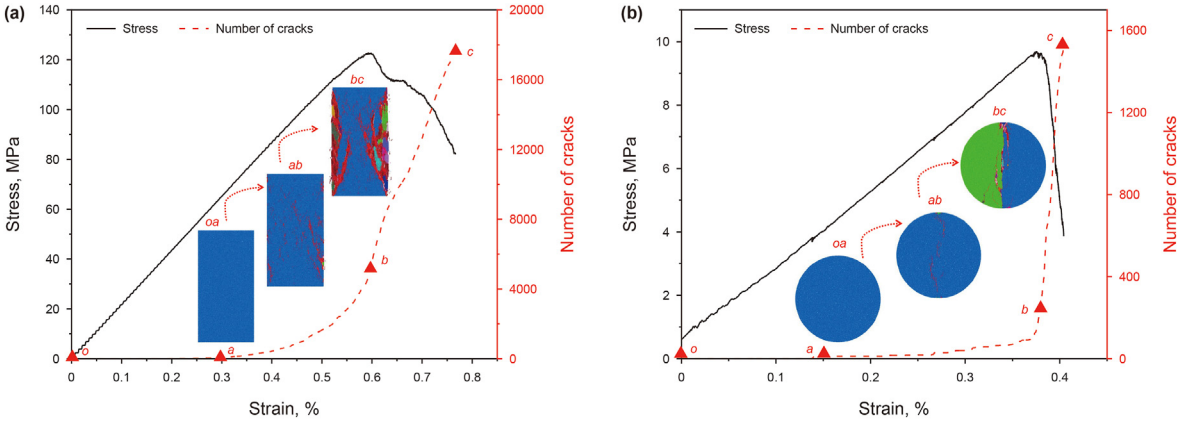

Fig. 15. Calibration of parameters.

Table 1
The calibrated microscopic parameters of granite.

Micro-parameters	Value				
Minerals properties	Quartz	Plagioclase	Orthoclase	Mica	Grain boundary properties
Minimum particle radius, mm	0.075	0.075	0.075	0.075	–
Particle-size ratio	1	1	1	1	–
Particle density, kg/m^3	2700	2700	2700	2700	–
Contact normal to shear stiffness ratio	3	3	2.0	0.9	–
Particle-particle contact modulus, GPa	17.26	15.918	11.836	6	–
Particle friction coefficient	0.5	0.5	0.5	0.5	0.5
Radius multiplier	2	2	2	1.75	2
Parallel bond normal to shear stiffness ratio	3	3	2	0.9	1
Parallel bond modulus, GPa	17.26	15.918	11.836	6	–
Contact normal stiffness, N/m	–	–	–	–	8e12
Contact tensile strength, N/m	–	–	–	–	2e12
Parallel bond tensile strength, MPa	22	20.95	21.56	20.68	5.5
Parallel bond cohesion, MPa	48	45.6	47.04	45.12	35
Parallel bond friction angle, °	72	72	72	72	75

Table 2
The comparison between experimental results and simulation results.

Parameters	Experimental value	Simulation value	Error, %
Tensile strength, MPa	9.11	9.67	6.15
UCS, MPa	117.4	122.77	4.57
Elastic modulus, GPa	21.5	20.83	3.1

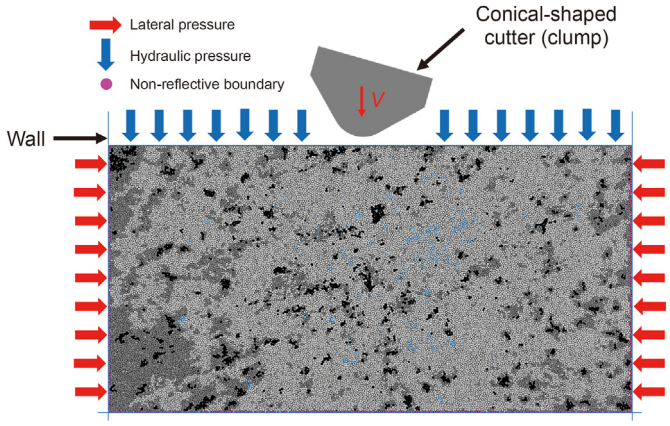

Fig. 16. Single cutter impact granite model.

addition, the number of cracks, *k*, and the volume of cuttings are also decreasing. It can be seen that the lateral pressure inhibits the rock breaking by suppressing the expansion of the radial crack.

5.3. Effect of hydraulic pressure on the rock-breaking mechanism

Fig. 21 shows the crushing results of granite impacted by the cutter with an energy of 60 J under different hydraulic pressures. Under hydraulic pressures, the radial crack propagation is promoted, while the transverse crack propagation is restrained, which leads to the reduction of rock cuttings volume. With the increase of hydraulic pressure, the number of cracks decreases, and the value of m increases. However, the hydraulic pressure has little effect on the value of k. It can be seen that the hydraulic pressure inhibits rock breaking by suppressing the propagation of the transverse crack.

5.4. Effect of confining pressure on the rock-breaking mechanism

Under confining pressure, the impact rock-breaking simulation with the cutter under the energy of 60 J was carried out, as shown in Fig. 22. With the increase of confining pressure, the cuttings volume and the value of L_r decreased, while the value of m increases, and the value of k changes little, which is similar to the situation under hydraulic pressure, indicating that hydraulic pressure plays a dominant role in confining pressure.

6. Conclusions

In this study, the impact rock-breaking experiments by four kinds of PDC cutters are carried out using a drop-weight impact testing machine and an AE recording system. This study also includes a numerical simulation to examine the process of crack initiation, propagation, and cuttings formation during the impact process with the consideration of confining pressure. The main conclusions are as follows.

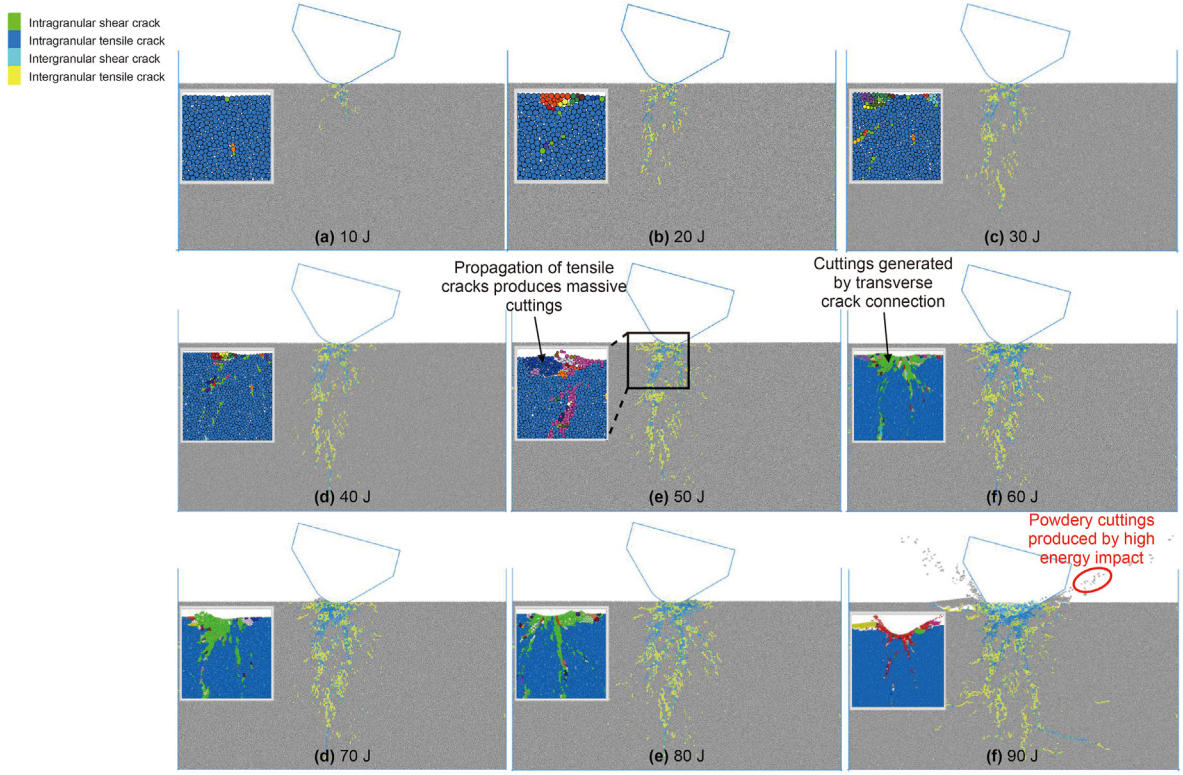

Fig. 17. Rock breaking with different energies at atmospheric pressure.

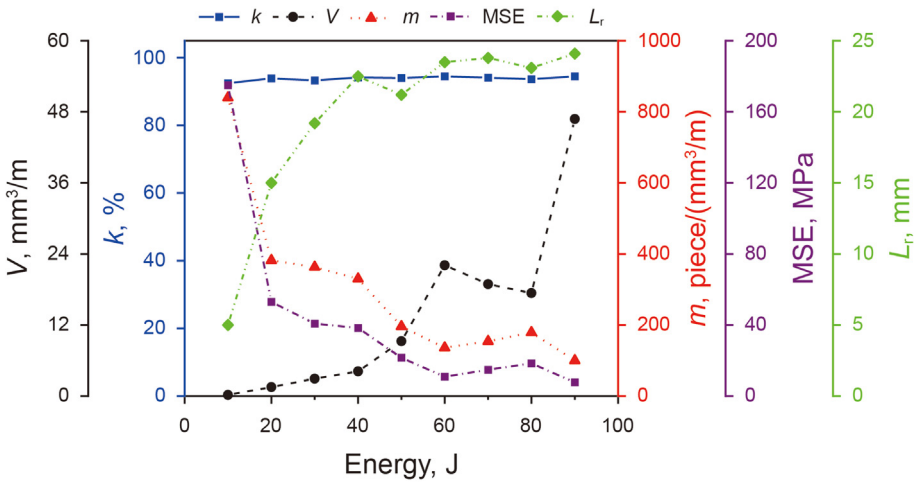

Fig. 18. Rock-breaking efficiency with different energies at atmospheric pressure.

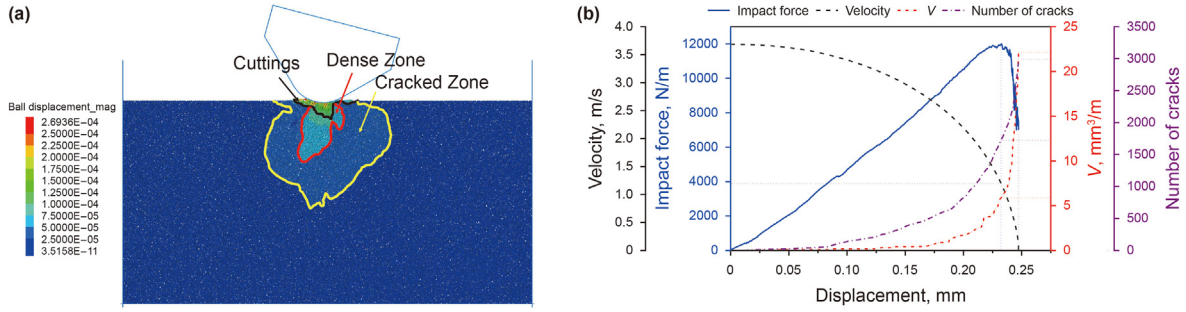

Fig. 19. Simulation of single cutter impact on granite under 60 J impact energy at atmospheric pressure. (**a**) Rock fragmentation under the impact, (**b**) Variation curves of impact force, velocity, cuttings volume, and crack number with displacement.

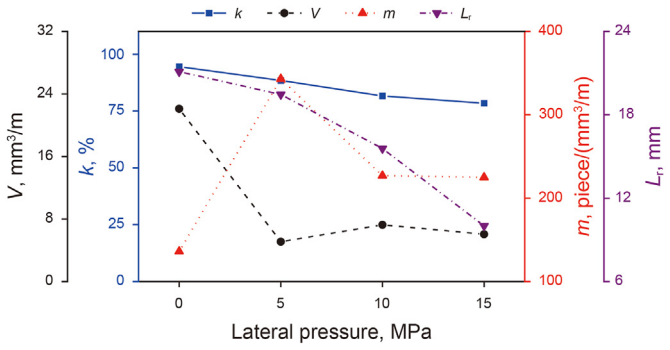

Fig. 20. Effect of lateral pressure on cuttings volume and crack propagation.

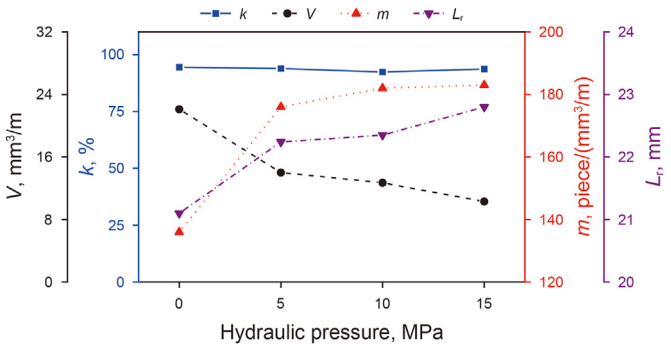

Fig. 21. Effect of hydraulic Pressure on cuttings volume and crack propagation.

1. Among the cylindrical cutters, Ax-shaped cutters, conical-shaped cutters, and three-blade cutters, the conical-shaped cutter is the most aggressive with high breaking efficiency. The penetration depth of the cutter is mainly affected by the impact energy and shape of the cutter. In comparison, the rake angle of the cutter has little effect on the penetration depth.
2. There exists a critical impact energy that makes the rock-breaking efficiency the highest. When using the conical-shaped cutter with a rake angle of 15° under atmospheric pressure, the critical impact energy is about 40 J.
3. The results of AE and numerical simulation show that the rock mainly failed in tensile mode, and inter-grain cracks are the main cracks.
4. Compared with GBM, E-PBM can better capture the failure of heterogeneous hard rock under impact. Hydraulic pressure will suppress the formation of horizontal cracks, while lateral

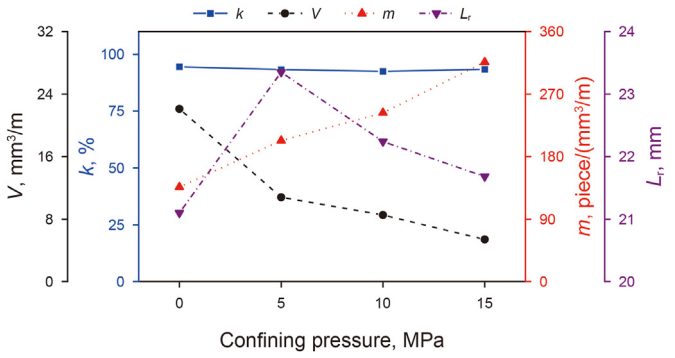

Fig. 22. Effect of confining pressure on cuttings volume and crack propagation.

pressure can inhibit the extension of vertical cracks and reduce the proportion of tensile cracks.

Declaration of competing interest

This paper is new, neither the entire paper nor any part of its content has been published or has been accepted elsewhere. It is not being submitted to any other journal. All authors have seen the manuscript and approved to submit to your journal.

Acknowledgments

This study is supported by the National Natural Science Foundation of China (Grant No.52034006, No.52004229, No.52225401, No.52274231), Regional Innovation Cooperation Project of Sichuan Province (2022YFQ0059), Science and Technology Cooperation Project of the CNPC-SWPU Innovation Alliance (2020CX040301), Natural Science Foundation of Sichuan Province (23NSFSC 2099), Science and Technology Strategic Cooperation Project between Nanchong City and Southwest Petroleum University (SXHZ004). Such supports are greatly appreciated by the authors.

References

Ajibose, O.K., Wiercigroch, M., Akisanya, A.R., 2015. Experimental studies of the resultant contact forces in drillbit–rock interaction. Int. J. Mech. Sci. 91, 3–11. https://doi.org/10.1016/j.ijmecsci.2014.10.007.

Aldannawy, H.A., Gerbaud, L., Rouabhi, A., 2021. On the Influence of Tool Shape on Percussive Drilling in Hard Rocks 55th U.S. Rock Mechanics/Geomechanics Symposium. Paper No. ARMA-21–1145. https://onepetro.org/ARMAUSRMS/proceedings-pdf/ARMA21/All-ARMA21/ARMA-2021-1145/2479135/arma-2021-1145.pdf.

Bahrani, N., Kaiser, P.K., Valley, B., 2014. Distinct element method simulation of an analogue for a highly interlocked, non-persistently jointed rockmass. Int. J. Rock Mech. Min. Sci. 71, 117–130. https://doi.org/10.1016/j.ijrmms.2014.07.005.

Du, H., Dai, F., Liu, Y., et al., 2020. Dynamic response and failure mechanism of hydrostatically pressurized rocks subjected to high loading rate impacting. Soil Dynam. Earthq. Eng. 129, 105927. https://doi.org/10.1016/j.soildyn.2019.105927.

Han, Z., Zhou, J., Zhang, L., 2018. Influence of grain size heterogeneity and in-situ stress on the hydraulic fracturing process by PFC2D modeling. Energies 11, 1413. https://doi.org/10.3390/en11061413.

Huang, L., Liu, J., Zhang, F., et al., 2019. Exploring the influence of rock inherent heterogeneity and grain size on hydraulic fracturing using discrete element modeling. Int. J. Solid Struct. 176–177, 207–220. https://doi.org/10.1016/j.ijsolstr.2019.06.018.

Hustrulid, W.A., Fairhurst, C., 1971. A theoretical and experimental study of the percussive drilling of rock Part II—force-penetration and specific energy determinations. Int. J. Rock Mech. Min. Sci. Geomech. Abstracts 8 (4), 335–356. https://doi.org/10.1016/0148-9062(71)90046-5.

Ji, Z., Shi, H., Dai, X., et al., 2021. Fragmentation characteristics of rocks under indentation by a single polycrystalline Diamond Compact cutter. J. Energy Resour. Technol. 143 (10), 100903. https://doi.org/10.1115/1.4050340.

Jiang, H., Cai, Z., Wang, O., et al., 2020. Experimental and numerical investigation of rock breakage by indenter impact. Shock Vib. 2020, 2747830. https://doi.org/10.1155/2020/2747830.

Jiang, J., Su, G., Yan, Z., et al., 2022. Rock crack type identification by Gaussian process learning on acoustic emission. Appl. Acoust. 197, 108926. https://doi.org/10.1016/j.apacoust.2022.108926.

Li, H., Liu, S., Chang, H., 2020. Experimental research on the influence of working parameters on the drilling efficiency. Tunn. Undergr. Space Technol. 95, 103174. https://doi.org/10.1016/j.tust.2019.103174.

Li, Y., Peng, J., Zhang, P., et al., 2021. Hard rock fragmentation in percussion drilling considering confining pressure: insights from an experimental study. Int. J. Rock Mech. Min. Sci. 148, 104961. https://doi.org/10.1016/j.ijrmms.2021.104961.

Liu, H., Kou, S., Lindqvist, P.A., 2008. Numerical studies on bit-rock fragmentation mechanisms. Int. J. GeoMech. 8 (1), 45–67. https://doi.org/10.1061/(ASCE)1532-3641(2008)8:1(45).

Liu, W., Zhu, X., Jing, J., 2018a. The analysis of ductile-brittle failure mode transition in rock cutting. J. Petrol. Sci. Eng. 163, 311–319. https://doi.org/10.1016/j.petrol.2017.12.067.

Liu, W., Zhu, X., Li, B., 2018b. The rock breaking mechanism analysis of rotary percussive cutting by single PDC cutter. Arabian J. Geosci. 11 (9), 192. https://doi.org/10.1007/s12517-018-3530-6.

Meng, F., Wong, L.N.Y., Zhou, H., 2021. Rock brittleness indices and their applications to different fields of rock engineering: a review. J. Rock Mech. Geotech. Eng. 13 (1), 221–247. https://doi.org/10.1016/j.jrmge.2020.06.008.

Meng, F., Zhou, H., Zhang, C., et al., 2015. Evaluation methodology of brittleness of rock based on post-peak stress-strain curves. Rock Mech. Rock Eng. 48 (5), 1787–1805. https://doi.org/10.1007/s00603-014-0694-6.

Oparin, V.N., Karpov, V.N., Timonin, V.V., et al., 2022. Evaluation of the energy efficiency of rotary percussive drilling using dimensionless energy index. J. Rock Mech. Geotech. Eng. 14 (5), 1486–1500. https://doi.org/10.1016/j.jrmge.2021.12.021.

Pavlovskaia, E., Hendry, D.C., Wiercigroch, M., 2015. Modelling of high frequency vibro-impact drilling. Int. J. Mech. Sci. 91, 110–119. https://doi.org/10.1016/j.ijmecsci.2013.08.009.

Potyondy, D.O., Cundall, P.A., 2004. A bonded-particle model for rock. Int. J. Rock Mech. Min. Sci. 41 (8), 1329–1364. https://doi.org/10.1016/j.ijrmms.2004.09.011.

Saadat, M., Taheri, A., Kawamura, Y., 2021. Investigating asperity damage of natural rock joints in polycrystalline rocks under confining pressure using grain-based model. Comput. Geotech. 135, 104144. https://doi.org/10.1016/j.compgeo.2021.104144.

Saadati, M., Weddfelt, K., Larsson, P.L., 2020. A spherical indentation study on the mechanical response of selected rocks in the range from very hard to soft with particular interest to drilling application. Rock Mech. Rock Eng. 53 (12), 5809–5821. https://doi.org/10.1007/s00603-020-02242-9.

Saksala, T., 2016. Numerical study of the influence of hydrostatic and confining pressure on percussive drilling of hard rock. Comput. Geotech. 76, 120–128. https://doi.org/10.1016/j.compgeo.2016.02.021.

Saksala, T., Fourmeau, M., Kane, P.A., et al., 2018. 3D finite elements modelling of percussive rock drilling: estimation of rate of penetration based on multiple impact simulations with a commercial drill bit. Comput. Geotech. 99, 55–63. https://doi.org/10.1016/j.compgeo.2018.02.006.

Saksala, T., Gomon, D., Hokka, M., et al., 2014. Numerical and experimental study of percussive drilling with a triple-button bit on Kuru granite. Int. J. Impact Eng. 72, 56–66. https://doi.org/10.1016/j.ijimpeng.2014.05.006.

Song, H., Shi, H., Yuan, G., et al., 2022. Experimental study of the energy transfer efficiency and rock fragmentation characteristics in percussive drilling. Geothermics 105, 102497. https://doi.org/10.1016/j.geothermics.2022.102497.

Song, X., Aamo, O.M., Kane, P.A., et al., 2021. Influence of weight-on-bit on percussive drilling performance. Rock Mech. Rock Eng. 54 (7), 3491–3505. https://doi.org/10.1007/s00603-020-02232-x.

Tan, P., Jin, Y., Pang, H., 2021. Hydraulic fracture vertical propagation behavior in transversely isotropic layered shale formation with transition zone using XFEM-based CZM method. Eng. Fract. Mech. 248, 107707. https://doi.org/10.1016/j.engfracmech.2021.107707.

Tan, X., Kou, S., Lindqvist, P.A., 1998. Application of the DDM and fracture mechanics model on the simulation of rock breakage by mechanical tools. Eng. Geol. 49 (3), 277–284. https://doi.org/10.1016/S0013-7952(97)00059-8.

Teng, M., Bi, J., Zhao, Y., et al., 2023. Experimental study on shear failure modes and acoustic emission characteristics of rock-like materials containing embedded 3D flaw. Theor. Appl. Fract. Mech., 103750 https://doi.org/10.1016/j.tafmec.2023.103750.

Wang, Y., Deng, H., Deng, Y., et al., 2021a. Study on crack dynamic evolution and damage-fracture mechanism of rock with pre-existing cracks based on acoustic emission location. J. Petrol. Sci. Eng. 201, 108420. https://doi.org/10.1016/j.petrol.2021.108420.

Wang, S., Zhou, J., Zhang, L., et al., 2021b. Parameter studies on the mineral boundary strength influencing the fracturing of the crystalline rock based on a novel Grain-Based Model. Eng. Fract. Mech. 241, 107388. https://doi.org/10.1016/j.engfracmech.2020.107388.

Xi, Y., Wang, W., Fan, L., et al., 2022. Experimental and numerical investigations on rock-breaking mechanism of rotary percussion drilling with a single PDC cutter. J. Petrol. Sci. Eng. 208, 109227. https://doi.org/10.1016/j.petrol.2021.109227.

Yang, Y., Zhang, C., Lin, M., et al., 2018. Research on rock-breaking mechanism of cross-cutting PDC bit. J. Petrol. Sci. Eng. 161, 657–666. https://doi.org/10.1016/j.petrol.2017.11.034.

Zhao, K., Ma, H., Liang, X., et al., 2022. Damage evaluation of rock salt under multilevel cyclic loading with constant stress intervals using AE monitoring and CT scanning. J. Petrol. Sci. Eng. 208, 109517. https://doi.org/10.1016/j.petrol.2021.109517.

Zhao, X., Elsworth, D., He, Y., et al., 2021. A grain texture model to investigate effects of grain shape and orientation on macro-mechanical behavior of crystalline rock. Int. J. Rock Mech. Min. Sci. 148, 104971. https://doi.org/10.1016/j.ijrmms.2021.104971.

Zhu, X., Chen, M., Liu, W., et al., 2022. The fragmentation mechanism of heterogeneous granite by high-voltage electrical pulses. Rock Mech. Rock Eng. 55 (7), 4351–4372. https://doi.org/10.1007/s00603-022-02874-z.

Zhu, X., Luo, Y., Liu, W., 2019. The rock breaking and ROP increase mechanisms for single-tooth torsional impact cutting using DEM. Petrol. Sci. 16 (5), 1134–1147. https://doi.org/10.1007/s12182-019-0318-6.